Atomistic modeling of the fracture of polycrystalline diamond

O. A. Shenderova and D. W. Brenner
North Carolina State University, Raleigh, North Carolina 27695

A. Omeltchenko and X. Su
Louisiana State University, Baton Rouge, Louisiana 70803

L. H. Yang
Lawrence Livermore National Laboratory, Livermore, California 94551
(Received 12 April 1999; revised manuscript received 2 September 1999)

A series of molecular-dynamics simulations using a many-body interatomic potential has been performed to investigate the behavior under load of several ⟨001⟩ and ⟨011⟩ symmetrical tilt grain boundaries (GB's) in diamond. Cohesive energies, the work for fracture, maximum stresses and strains, and toughness as a function of GB type are evaluated. Results indicate that special short-period GB's possess higher strengths and greater resistance to crack propagation than GB's in nearby misorientation angles. Based on dynamic simulations, it was found that the mechanism of interface failure for GB's without preexisting flaws is not that implied by Orovan's criterion, but rather GB strength is defined by GB type instead of cleavage energy. In simulations of crack propagation within GB's on the other hand, it was found that critical stresses for crack propagation from atomistic simulation and from the Griffith criterion are consistent, indicating that GB cleavage energy is an important characteristic of GB toughness. Crack propagation in polycrystalline diamond samples under an applied load was also simulated and found to be predominantly transgranular rather than intergranular.

I. INTRODUCTION

With strength values ranging between 180 and 5190 MPa, and fracture toughness between 5.3 and 8 $MN\,m^{-3/2}$,[1–8] chemical vapor deposited (CVD) diamond films have received considerable attention for applications requiring hard, wear-resistant coatings. Relationships between specific values for these properties, and microstructure and crack propagation mechanisms, however, are not well understood. This is largely due to the small size and relatively high cost of specimens, and the large variability in microstructure resulting from different deposition conditions. It is well established experimentally in metals[9,10] and ceramics[11] that certain types of grain boundaries can facilitate crack propagation, while others increase fracture toughness. This has led to the concept of grain boundary design[12] in which the fracture resistance of polycrystalline materials is optimized through the production of microstructures with an optimal distribution and arrangement of ''fracture-resistant'' boundaries. This concept could be applied to CVD diamond provided that the role of specific microstructural elements on crack propagation was better understood.

Atomistic modeling techniques have been used to estimate intergranular cohesion and theoretical fracture strengths.[13–15] These quantities can be determined for individual grain boundaries (GB's) using either frozen separation or slow straining methods.[14] In the frozen separation method two grains are pulled apart while maintaining relative atomic positions within the grains. The maximum stress determined in this way gives an upper bound for the fracture stress required to cleave a sample along a specific GB plane. In the slow straining method, the system is allowed to relax while gradually increasing the applied strain until total fracture occurs. This approach accounts for part of the plastic response of the GB to the work for fracture, that can be computed from the area under a stress-strain curve.

Atomistic simulations have also provided important insights into the mechanisms of crack propagation,[16] and have linked atomic-scale concepts to the Griffith condition for failure in systems with preexisting flaws.[17] The first atomistic simulations of crack propagation were carried out in the early 1970s using model systems representing bcc and fcc metals, and diamondlike materials.[18–20] More recently, large-scale atomistic simulations of crack propagation in more complicated systems and microstructures have been carried out. These have included, for example, a bicrystal,[21] nanocrystalline solids,[22] notched graphene,[23] and other more complicated networks of grains and grain boundaries.[24]

In the present paper, results from a series of molecular-dynamics simulations designed to yield insight into the relationship between microstructural elements and the fracture properties and crack propagation mechanisms in polycrystalline diamond are reported. The fracture properties of individual ⟨001⟩ and ⟨011⟩ symmetrical tilt GB's both with and without preexisting flaws are studied in several sets of simulations. The simulations predict that special short-period GB's possess higher strengths than GB's in the nearby misorientation range, consistent with their enhanced energetic stability. The simulations also predict that crack propagation in notched samples is primarily transgranular unless an initial crack is inserted directly into a GB. Finally, crack propagation is modeled through a system containing a set of microstructural elements chosen to model pieces of experimentally observed microstructures in CVD diamond films. The simulations show both transgranular and intergranular crack propagation depending on the cleavage en-

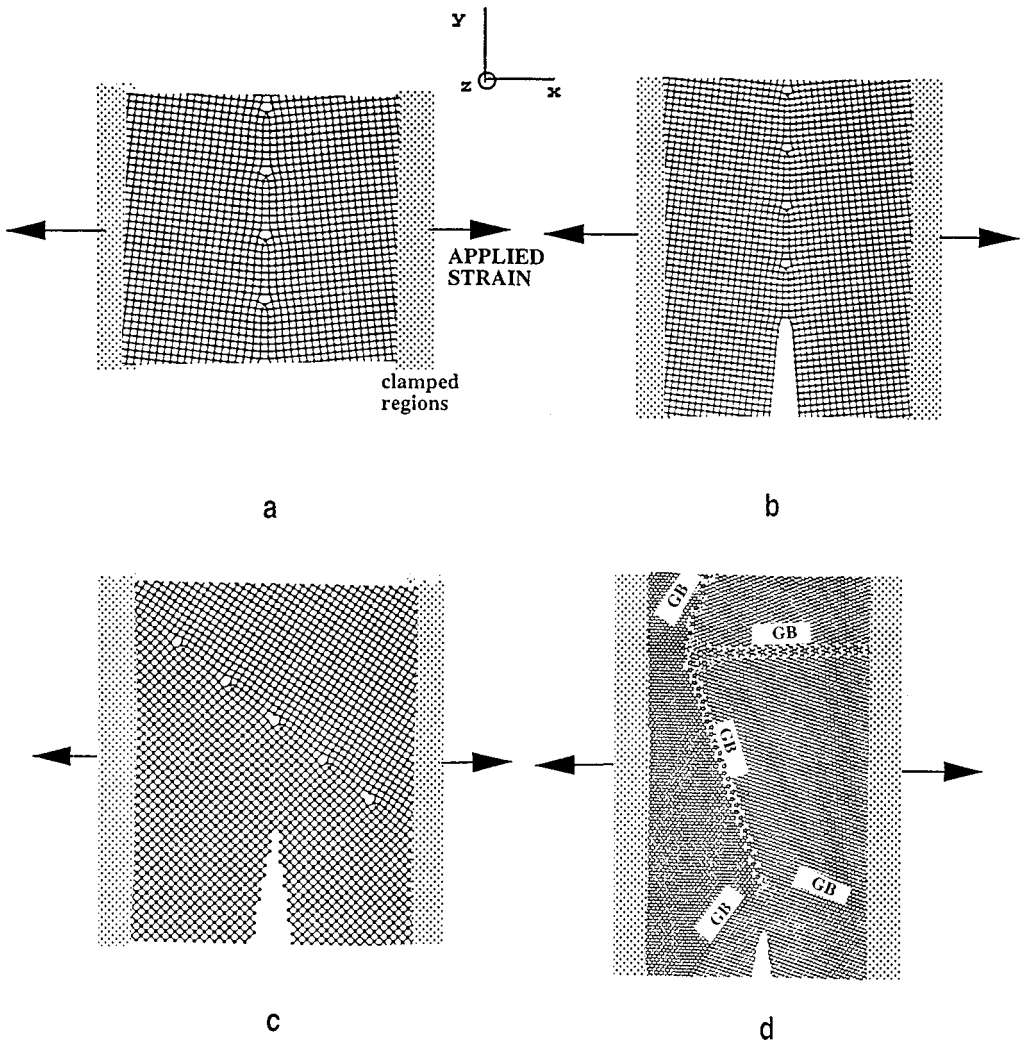

FIG. 1. Illustrations of the simulated systems. (a) Simulation setup for modeling the fracture strengths of individual GB's; (b) system for modeling intergranular crack propagation; (c) crack propagation at different initial orientations between a notch and GB plane; (d) crack propagation in a microstructure with realistic features.

ergy and the grain boundary orientation with respect to the applied strain.

II. CALCULATIONAL METHODS

Four sets of simulations, each with a different type of initial structure, were considered. The first set consisted of single symmetrical tilt GB's with ⟨001⟩ and ⟨011⟩ misorientation axes with no preexisting flaws. The initial structures of these GB's are based on a coincident-site lattice model for group-IV materials in which each atom is fourfold coordinated.[25] To estimate theoretical strengths, the crystals were strained at a rate of 1% ps along the direction perpendicular to the GB plane [Fig. 1(a)]. This was accomplished by moving two regions of atoms 3 Å wide and 10 lattice parameters on either side of the GB away from the interface. During strain, the atomic positions within the end regions were held constant while the remaining atoms were allowed to move by integrating classical equations of motion using forces from the analytic potential discussed below. Periodic boundary conditions were maintained within the GB plane, and each system contained approximately 4000 atoms. The quantities considered in this set of simulations were the maximum fracture stresses of the GB's compared to the bulk, and the GB work for fracture, which characterizes the ability of the material to adsorb energy without failing.

The structures examined in the second set of simulations consisted of crystals in which a surface notch 30 Å long oriented perpendicular to the direction of strain was inserted into the GB [Fig. 1(b)]. Strain was applied to these systems as described above until a crack started to propagate, after which the coordinates of the atoms in the end regions were left unchanged. Periodic boundary conditions were applied along the z axes only (see Fig. 1 for the axis orientation), and the simulations were performed for several $80\times180\times20$ Å diamond samples, each of which contained approximately 50 000 atoms. The third set of simulations was identical to the second except that different GB orientations with respect to the notch and applied strain were examined. These were carried out so that both transgranular and intergranular crack propagation could be modeled [Fig. 1(c)].

In the final type of simulation, crack propagation in a more complicated polycrystalline microstructure containing five ⟨011⟩ tilt GB's and two triple junctions was simulated. The microstructure used in this simulation, which is illus-

TABLE I. Properties of diamond given by the analytic bond-order potential, DFT/LDA calculations and experiments.

Property	Analytic Potential	DFT/LDA	Experiment
Lattice constant (Å)	3.566	3.52	3.566[a]
Bulk modulus (Mbar)	4.45	4.62	4.44[a]
Shear modulus (Mbar)	5.4	5.2	5.0–5.5[b]
C_{11} (Mbar)	10.78	11.11	10.81[a]
C_{12} (Mbar)	1.31	1.38	1.25[a]
C_{44} (Mbar)	6.8	5.95	5.79[a]

[a]From Ref. 30.
[b]From Ref. 1.

trated in Fig. 1(d), was constructed to mimic that observed experimentally in CVD diamond.[26] All atoms in the structure are four-fold coordinated, and there are no cavities between the grains. To construct this system, two triple junctions having a common $\Sigma=9$ GB were first connected to one another along this GB. The system size was then increased by translating other sections of the crystal to the open regions. The final system had dimensions $150\times260\times20$ Å contained 120 000 atoms and was periodic in the z direction. Details of the atomic structures of the $\Sigma9=\Sigma3(111)+\Sigma3(111)$ and $\Sigma27=\Sigma9+\Sigma3(211)$ triple junctions are described elsewhere.[27]

A reactive analytic bond-order potential was used to model the interatomic forces. This formalism, which is based on the second moment approximation to the local electronic density of states, models the interatomic energy as a sum of repulsive and attractive pair potentials. The attractive pair terms, which model bonding from the valence electrons, are modulated by analytic bond order functions whose values depend on coordination, bond angles, radical character of the bond, and an approximation to conjugation effects arising from adjacent unsaturated atoms. The form of the potential is similar to that in Ref. 28 with two modifications. The first is a slightly different set of functional forms for the pair terms and the bond-order function[29] that better describe the elastic properties of diamond compared to those given in Ref. 28. These properties are listed in Table I along with corresponding experimental data. The second modification, described below, is related to the cut-off function used to restrict the potential to nearest neighbor interactions.

Fracture simulations provide a stringent test of the reliability of interatomic potentials because fracture properties are not usually included in a fitting database. During crack propagation, atoms are subjected to different bonding environments where the high strain near a crack tip results in atomic configurations that are far from their ideal bond lengths and bond angles. In particular, fracture properties are sensitive to the behavior of the interatomic potential near an inflection point. In the scheme of nearest-neighbor interatomic potentials, which are typical for describing bonding in covalent materials, the interaction must be cut off before the second neighbor distance using a suitable switching function. The form of the switching function need not influence most of the bulk and surface properties of materials and therefore is usually chosen arbitrarily rather than fit to some physical property. However, the switching function is crucial for describing bond breaking during the fracture process; arbitrary switching functions can therefore result in nonphysical behavior in atomistic fracture simulations. In preliminary simulations, for example, it was found that the influence of a switching function on the inflection point of the interatomic potential can result in very high stresses and strains required for diamond fracture.[31]

In the initial version of the potential,[28] a switching function cuts off the interaction between 1.7 and 2.0 Å. This nearest-neighbor bonding model for carbon is well justified by the nature of covalent bonding and works well for most equilibrium structures. However, the fixed switching function approach is problematic as C-C bonds are stretched beyond 1.7 Å because it significantly influences the forces in the vicinity of the inflection point ($\sim$1.85 Å in diamond for the $\langle111\rangle$ direction). To avoid this problem in the present study, the cutoff distance was extended far beyond the inflection point. To preserve the nearest-neighbor character of interactions, a bond list using the original (2 Å) cutoff distance was constructed for the initial system that was left unchanged during the simulations. This *ad hoc* scheme solves the cutoff problem while still describing bond breaking and changes in the chemistry of the bond during cleavage (e.g., formation of double, triple, and conjugated bonds). However, its application is restricted to phenomena that involve bond breaking and rehybridization, but not new bond formation.

It is well established[17] that the area bounded by the curve of stress as a function of the separation between atomic planes up to the maximum stress should approximately equal the surface energy γ. With the modified cutoff procedure, this area calculated for separation of (111) diamond planes is about 0.85γ, which is very reasonable. The calculated maximum tensile strength for bond breaking in the $\langle111\rangle$ direction is 96 GPa, which is close to the value calculated by Tyson[32] using atomic force constants. These tests demonstrate the reliability of the interatomic potential for simulating fracture.

III. RESULTS AND DISCUSSIONS

In subsection A below, analysis of GB cohesion based on energetic considerations is discussed, followed in subsection B by the results of molecular dynamic simulations of cleavage of individual GB's. The first purpose of these calculations is to determine the extent to which GB strengths *calculated* using GB cohesion energies (via Orovan's criterion, for example) are consistent with those obtained from molecular-dynamics *simulations*. The second purpose of these calculations is to determine the types of GB's having relatively high strengths. In the final subsection results on the crack behavior in the material containing GB's are presented. Of primary interest is to determine if critical stresses of the intergranular crack propagation *calculated* with the Griffith criterion (using GB cohesion energies) are consistent with those obtained in the dynamic *simulations*. The inter- versus transgranular crack propagation in diamond is also discussed.

A. Grain boundary cohesion

The energy required to cleave a brittle material along a GB plane without plastic deformation is defined through the relation[17]

TABLE II. Grain boundary theoretical strength properties, calculated from molecular dynamics simulations for ⟨001⟩ and ⟨011⟩ symmetrical tilt GB's (STGB). The ratio W_{GB}/W_{111} is the relative work for fracture. Cohesive energies were calculated both with DFT/LDA method and using the bond order potential (BOP)

θ degrees	boundary plane	Young's Modulus (GPa)	Maximum Stress (GPa)	Maximum Strain (%)	W_{GB}/W_{111}	Cohesive Energy (J/m^2) BOP	DFT-LDA
	(111)	1100	96	15.1	1.0	10.8	13.4
				⟨001⟩ STGB:			
0.0	(110)	1000	115	19.2	1.30	6.7(10.9[a])	11.2
12.68	(450)	900	52	8.9	0.29	4.7	8.7
20.01	(7 10 0)	830	53	7.5	0.26	5.2	8.9
36.87	(120)	810	62	10.5	0.42	8.6	11.1
53.13	(130)*S*	800	73	14.8	0.67	11.0	12.9
	(130)*Z*	800	69	13.7	0.57	11.2	13.0
73.74	(170)	730	46	8.3	0.23	13.2	13.2
90.0	(100)	850	90	24.0	1.60	22.0	18.6
				⟨011⟩ STGB:			
13.44	(166)	860	50	7.6	0.23	4.1	
31.59	(255)	910	58	8.8	0.34	7.8	
38.94	(122)	940	62	9.2	0.37	9.1	

[a]Cohesive energy of (110) surface calculated with Griffith formula using critical stresses obtained from dynamic simulations.

$$E_{\text{cohesion}} = \gamma_1 + \gamma_2 - E_{gh}, \quad (1)$$

where γ_1, γ_2 are energies of the two unreconstructed surfaces created due to cleavage and E_{gb} is the GB energy (E_{gb} is zero for bulk cohesion). In diamond, where plastic deformation is negligible and therefore Eq. (1) may be applied, it is expected that calculated GB cohesive energies will give reasonable estimates for the relative strengths of grains and grain boundaries.

Summarized in Table II and plotted in Fig. 2 are GB cohesive energies for ⟨001⟩ symmetrical tilt GB's as a function of misorientation angle θ. Surface energies were calculated for a few surface orientations and then extrapolated through the entire misorientation range. The GB energies, which are necessary for calculating GB cleavage energies, were evaluated over the entire range of misorientation angle using a multiscale modeling approach that combines continuum and atomic-level models.[33] The relations in Fig. 2(a) were obtained from density-functional calculations using the local-density approximation (DFT/LDA). Details of these calculations are given elsewhere.[33] Plotted in Fig. 2(b) are the same curves calculated with the analytic bond-order potential described above. Although the cleavage energies are overall lower for the analytic potential compared to the first-principles DFT/LDA calculations, the relative energies for grain boundary and bulk cleavage are similar for the two methods. Cleavage energies of most ⟨001⟩ and ⟨011⟩ tilt GB's (Table II) are about 60–75 % of those for the ideal bulk crystals with the same orientation. It is also apparent from Fig. 2 and Table II that special short-period GB's [$\Sigma = 5(120)$, $\Sigma = 5(130)$ for ⟨001⟩ tilt axes and $\Sigma = 9(122)$ GB for ⟨011⟩ tilt axes] possess higher cleavage energies relative to GB's in the nearby misorientation range. Calculated GB cleavage energies will be used in the section B for evaluation of GB theoretical strengths that then will be compared with the GB strengths obtained from dynamic simulations.

Another important issue is the relative bulk cleavage energies of different low-index planes in diamond, which has been widely discussed in the literature on mechanical properties of diamond.[1,2] Our DFT/LDA calculations as well as those carried out by Kern and Hafner[34] using similar techniques predict that for diamond the (110) surface is energetically more stable than the unreconstructed (111) (1×1) surface for both relaxed and unrelaxed structures. This result is contrary to earlier reports on the mechanical properties of diamond.[1] The earlier calculations of surface energies were based on the evaluation of the energy of broken bonds per unit area of different surfaces. However, this does not account for the strong π bonding for carbon that leads to significant reduction of the energy of the (110) surface atoms due to the formation of π-bonded chains along the surface. Chain formation on the (110) surface is compatible with the geometry of the underlying lattice and does not require any surface reconstruction. Surface energies of (110) and unreconstructed (111) (1×1) diamond surfaces calculated within the DFT/LDA approach are 5.6 and 6.6 J/m^2, respectively.

To further illustrate the chemistry of the various surfaces, ball-and-stick models are given at the bottom of Fig. 2(a) that indicate the different bonding and defect types associated with atoms on surfaces within each misorientation interval. Atoms on the (100) surface (corresponding $\theta=90°$) possess two dangling bonds each. The (130) surface ($\theta=53.13°$) contains two types of atoms on which there are either one or two dangling bonds. The (120) surface ($\theta=36.87°$) contains atoms with two dangling bonds each and atoms forming π-bonded chains. Atoms on the (110) surface ($\theta=0°$) form π-bonded chains only. All free surfaces at angles intermediate between these delimiting angles contain a mix of the

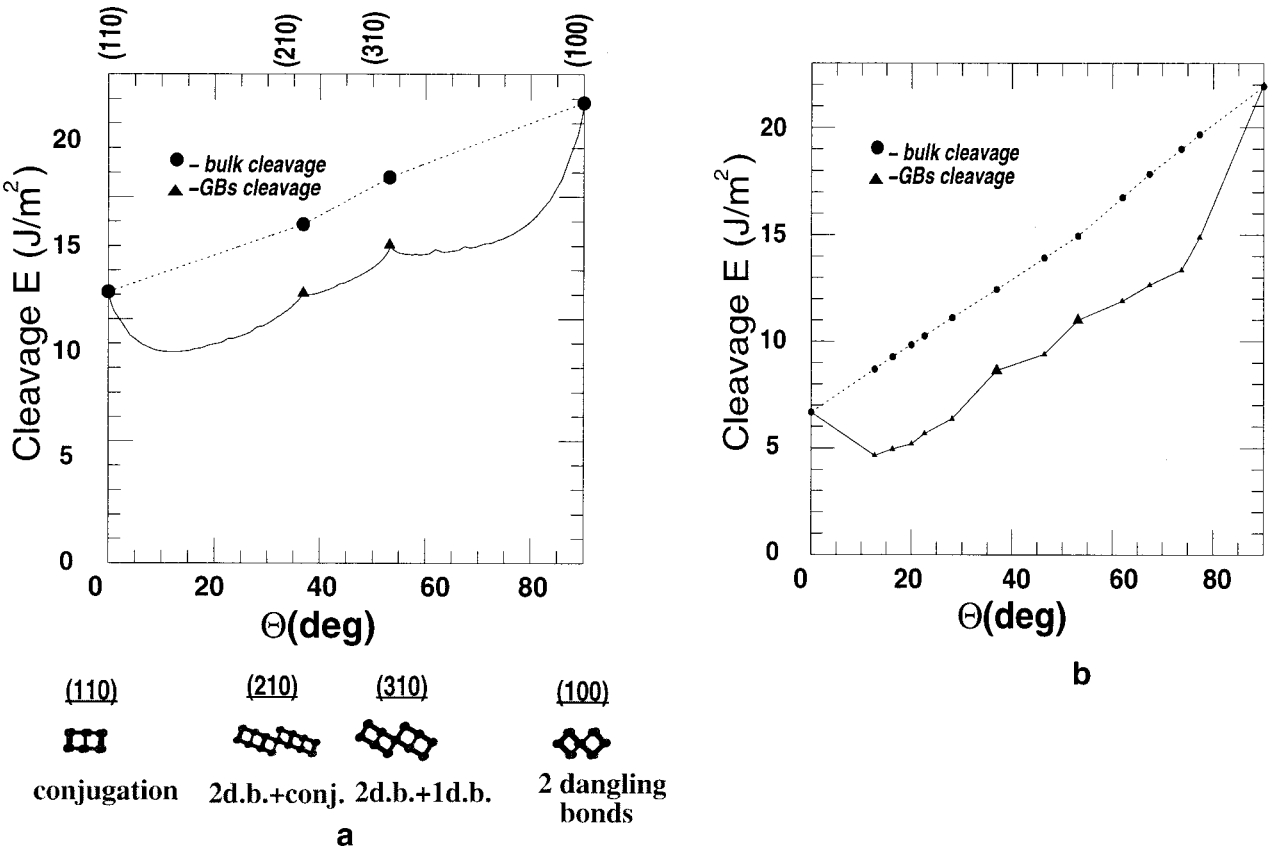

FIG. 2. Cleavage energies of ⟨001⟩ symmetrical tilt GB's in diamond. (a) Results from DFT/LDA calculations; (b) values calculated with the bond-order potential. For comparison, the bulk crystal cleavage energies are also shown.

bonding types of the delimiting surfaces. As a result, the curve of the dependence of surface energy on the misorientation angle consists of three straight lines with slightly different slopes (Fig. 2). In summary, the ''π-bonding chemistry'' should be taken into account when analyzing energetic characteristics of covalent materials with pronounced π bonding.

B. Dynamic simulation of theoretical strength

Below are discussed theoretical fracture characteristics (i.e., those for a sample with no preexisting cracks) obtained from molecular dynamics simulations for bulk diamond with low-index orientations and selected ⟨001⟩ and ⟨011⟩ symmetrical tilt GB's.

1. Ideal crystal strength

In the simulations using the slow straining method with the bond-order interatomic potential, the maximum tensile stress for the ⟨111⟩-oriented diamond is 96 GPa and the corresponding strain is 15.6%. For the frozen separation technique the maximum strength and strain are 5% and 20%, respectively, higher than those obtained in dynamic simulations. A variety of theoretical tensile strength values for ⟨111⟩-oriented diamond have been reported; these values range from 200 GPa (Ref. 35) (using Orovan's criterion) and 106 GPa (estimated assuming Morse-type interatomic interactions[32]) to 53 GPa (Ref. 36) (including third-order elastic coefficients). Thus, our value for maximum tensile stress for the ⟨111⟩-oriented diamond is closer to that reported by Tyson.[32]

It is well established experimentally that cleavage of diamond results in predominantly {111} planes.[1,2,37] Explanations of the preference for {111} cleavage were based on the consideration that most preferred cleavage would be that involving the least cleavage energy.[1] According to estimates of cleavage energies for diamond by Field,[1] cleavage should be along {111} planes. Another explanation involves the criterion of the least applied stress for cleavage along particular planes.[2] According to calculations by Whitlock and Ruoff,[36] the stress required to produce tensile fracture is minimal for the ⟨111⟩ direction (although for the ⟨011⟩ orientation reported the stress value is only slightly higher). In addition to the least fracture stress and least cleavage energy criteria, discussed above, further considerations regarding preferred cleavage planes may be developed. First, if critical stresses for cleavage for particular planes are close, the criterion of the least work for fracture might be involved for further analysis. The work for fracture characterizes the ability of the material to adsorb energy without fracture. In general, the work for fracture might exceed the cleavage energy since additional mechanisms of energy dissipation beyond pure bond breaking along the fracture plane during loading may appear. For example, the possibility of significant bond bending at loading along the ⟨001⟩ direction exists (and for ⟨011⟩ direction, too, although less pronounced) because at the given geometries the bonds make an angle with the axis of the applied strain. As a result for ⟨001⟩ and ⟨011⟩ orientations more strain may be relaxed by changing of bond angles as compared to the ⟨111⟩ crystal orientation. Another consideration regarding preference planes for cleavage in

diamond suggests that there can be planes of the preferential location of microdefects, which can serve as nuclei for microcracks. For example, it is known that {111} planes in CVD diamond contain a large amount of twins and stacking faults.[26] Finally, the most important characteristic defining a plane of preferred cleavage would be a critical stress for microcrack propagation, assuming that in-grown microcrack embryos are approximately of equal sizes in the possible cleavage planes. This case is discussed in section C. 1 of the present paper based on the dynamic simulation of microcracks using the bond order potential. However, to complete the analysis of the reason for very marked preference of {111} cleavage in diamond, further first-principles calculations are required to obtain least-critical stress values as well as the least work for fracture for low-index orientations from fracture dynamic simulations.

Based on the predicted DFT-LDA calculations of the bulk cohesive energies for the low-index orientations in diamond (Table II), it is evident that the least cleavage energy criterion does not explain the preferable cleavage along {111} planes since the cohesive energy for {011} planes is 17% lower. The dynamic simulations with the bond-order potential demonstrate that the critical fracture stress for ⟨011⟩-oriented diamond is 20% higher than for the ⟨111⟩ orientation even though the energy of the (011) surface is lower than that of the (111) surface. This is related to the fact that the potential predicts that π-bonded chains, which significantly decrease the surface energy, form primarily only after the interplane separation reaches the distance corresponding to the maximum stress. As a result, before the maximum stress is reached, the bonds behave as if they are purely single bonds. While physically plausible, accurate first-principles calculations of the fracture dynamics are required to further characterize simultaneous bond rupture and π-bonded chain formation during cleavage of a ⟨011⟩ oriented diamond crystal. Thus, the least critical tensile stress obtained with the bond-order potential, in principle, explains preferable cleavage for (111) planes as compared to (011) planes. Dynamic simulations with the bond-order potential also demonstrate that the work for fracture is 30% lower for (111) planes in comparison with (011) planes, and 60% lower than that for (001) planes (Table II). Thus, the least work for fracture for the (111) plane is also consistent with experimental observations.

It should also be noted that first-principles calculations suggest that the lowest energy among the low-index faces is for the reconstructed (111) surface[34] involving formation of seven-five member rings on the surface. If this surface reconstruction occurs simultaneously with bond breaking along the (111) surface, it could significantly decrease the work for fracture for the (111) plane. First principles calculations[34] also demonstrate that among low-index hydrogenated surfaces the (111) surface is more energetically stable. Thus atomic hydrogen can also, in principle, decrease the work for fracture for (111) planes.

2. Individual grain boundary strengths

Some typical stress-strain curves obtained from dynamic simulations of ideal diamond and systems containing GB's are illustrated in Fig. 3. The stress-strain curves for the short-period special $\Sigma=5(130)$ GB and the long-period $\Sigma=41(450)$ GB are shown in the figure. The fracture stresses and strains for the bicrystals are significantly lower than those for the ideal crystal.

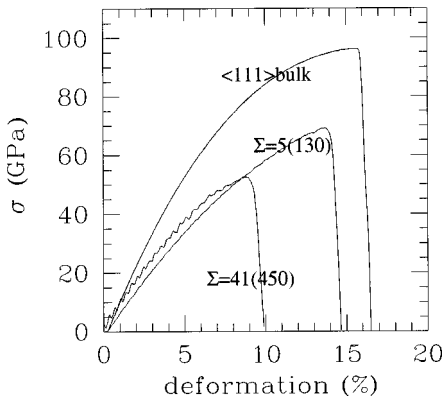

FIG. 3. Stress-strain curves for a ⟨111⟩-oriented ideal diamond sample and for samples containing $\Sigma=5(130)$ and $\Sigma=41(450)$ GB's.

Theoretical strength properties of different GB's with ⟨001⟩ and ⟨011⟩ misorientation axes estimated from the dynamic simulations are summarized in Table II and Fig. 4. Critical fracture stresses of samples with GB's are about 30–60 % lower than those for ideal diamond (Fig. 4, Table II). The work for fracture for various types of GB's is 40–80 % lower depending on the GB type than that for a ⟨111⟩ ideal diamond orientation (Table II).

The theoretical fracture stress of a crystal according to the Orovan criterion,[38] depends on the cleavage energy γ, Young's modulus E, and the interplanar spacing a_0 in the unstressed state of the planes perpendicular to the tensile axis through the relation

$$\sigma_{\max}=(E\gamma/a_0)^{1/2}. \tag{2}$$

This expression assumes that the energy required to break the bonds is provided by the stored elastic energy in the region nearby the fracture plane. Although it is well established that the magnitude of the ideal breaking strength is generally overestimated by Orovan's relation by up to a fac-

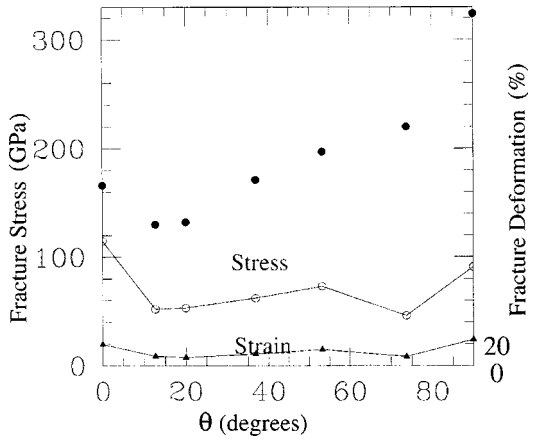

FIG. 4. Fracture stresses and strains of ⟨001⟩ tilt GB's in diamond. (a) Values obtained from molecular-dynamics simulations (open circles) and fracture stresses evaluated from the Orovan criterion (solid circles).

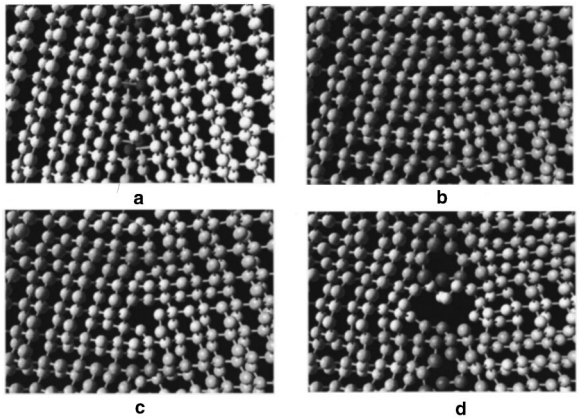

FIG. 5. Close up view of fracture initiation and propagation within the $\Sigma=25(340)$ GB in diamond.

tor of two,[35] the Orovan criterion has nonetheless been used to investigate the relationship between maximum stress and cleavage energies of GB's. Fracture stresses of GB's calculated with the Orovan criterion are given in Fig. 4. The quantitative difference between the results of atomic simulations and the analytic approach is not surprising. However, as can be seen from Fig. 4, there is little qualitative correlation between maximum stresses calculated from Orovan's criterion and those obtained from dynamic simulations. This is due to the specific mechanism of fracture initiation within a GB. At the critical local stress (which is several times higher than the applied stress), nucleation of microcracks occur within the dislocation cores at the GB that are initially under tension [Figs. 5(a) and 5(b)]. This is followed by bond breaking along the interface [Figs. 5(c) and 5(d)]. Thus Orovan's criterion cannot be used to accurately estimate theoretical strengths for GB's in diamond because of the *nonuniformity* of the cleavage energy distribution along the interface.

Structures of the surfaces after cleavage are illustrated in Fig. 6. Fracture surfaces for the $\Sigma=5(013)$ GB are rougher than those of higher Σ GB's. This indicates a higher work for fracture for the $\Sigma=5(013)$ GB in accordance with results in Table I. Thus, critical local stresses rather than GB cleavage energies define theoretical strengths of different types of GB's. Evidently, the maximum local stress depends on the intrinsic stresses in the vicinity of a GB that is enhanced by external stress when load is applied. Additional analysis is required to establish the correlation between the critical local stresses, applied load, and GB structure that defines the intrinsic GB stress.

It can be concluded that the relative theoretical strength of a GB is determined by its type. For example, these simulations have shown that certain short-period $\langle 001\rangle$ symmetrical tilt GB, namely the $\Sigma=1$ ($\theta=0°$ and $90°$), $\Sigma=5(012)(\theta=36.87°)$, and $\Sigma=5(013)(\theta=53.13°)$, possess about a 30% higher critical stress and 30% higher work for fracture than GB's in the nearby misorientation range (Table II, Fig. 4). Fracture strength is also higher for the special $\Sigma=9(122)$ GB than for other two GB's ($\Sigma=27$ and $\Sigma=81$) with $\langle 011\rangle$ tilt axes, which were also studied (Table II). This result is consistent with physical properties of special GB's in metals and ceramics that can be significantly different from those for other GB's in the nearby misorientation range.[15,39]

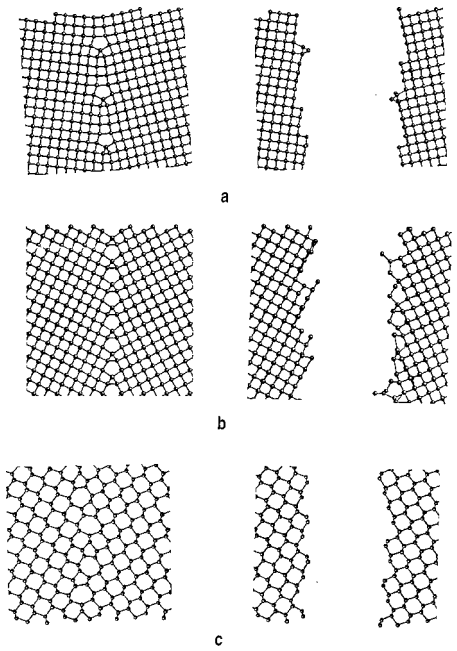

FIG. 6. Surface structures after cleavage. (a) Cleavage along the $\Sigma=149(7100)$ GB; (b) cleavage along the $\Sigma=5(013)$ GB; (c) cleavage along the $\Sigma=27(255)$ GB.

C. Crack propagation

1. Ideal crystals

As it was outlined above, the (111) plane is the experimentally preferred cleavage plane in diamond,[1] although other cleavage facets have been also observed,[37] particularly the (110) plane. Because diamond is a brittle material, it is expected that the Griffith criterion can predict relatively accurate critical stresses for bulk cleavage for samples with pre-existing cracks. Prior estimates of surface energies[1] from simple bond-scission analyses suggest that the (111) surface has the lowest surface energy followed by the (110) and (100) surfaces, respectively. Based on this cleavage energy ranking for low-index facets, from the Griffith criterion it follows that the critical stress of a crack propagation is minimal for the (111) plane, what corresponds to the experimental observations. However, as it was discussed above, simple bond-scission evaluations are inconsistent with the surface energies obtained from the DFT-LDA calculations as well as using the bond-order potential (see Table II). The critical stresses calculated from the Griffith equation using surface energies and elastic properties from the analytic potential are reported in Table III. These values predict a 23% higher critical stress for crack propagation along the (111) plane compared to the (110) plane. This trend is maintained with surface energies taken from the DFT/LDA calculations (see Table III).

To explore the reason for the discrepancy between the experimentally observed cleavage planes and the predicted critical stresses from the Griffith criterion in Table III, simulations of crack propagation within (111), (110), and (100) planes were performed. The model system for this set of calculations is illustrated in Fig. 1(b). The simulations yielded critical stresses for the (110) and (100) surfaces that are 4% and 15% higher, respectively, than that for the (111) surface. This is consistent with experiment, but inconsistent

TABLE III. Critical stresses for intergranular crack propagation of an initial crack 30 Å long obtained from molecular dynamic simulations with the bond order potential (σ_{MD}) and calculated from the Griffith criterion using cleavage energies obtained with the bond-order potential ($\sigma_{G(BOP)}$) and DFT-LDA calculations ($\sigma_{G(LDA)}$); toughness calculated from BOP cleavage energies $K_c=(2E\gamma)^{1/2}$, toughness from dynamic simulations $K_{MD}=\sigma_{MD}(\pi l)^{1/2}$

θ degrees	Σ	Boundary plane	σ_{MD} (GPa)	$\sigma_{G(BOP)}$ (GPa)	$\sigma_{G(LDA)}$ (GPA)	K_c (MN/m$^{3/2}$)	K_{MD} (MN/m$^{3/2}$)
	1	(111)	44	51	54	5	4.3
			⟨001⟩ STGB:				
0.0	1	(110) ⟨001⟩	46(48)[a]	37	48	3.7	4.3
		(110) ⟨011⟩	50(56)[b]	37			
12.68	41	(450)	27	29	39	2.8	2.6
36.87	5	(120)	46	37	42	3.6	4.5
53.13	5	(130)*S*	54	42	46	4.1	5.2
		(130)*Z*	36	42	45	4.1	3.5
	bulk	(130)	50[c]	53		5.1	4.9
73.74	25	(170)	38	44	44	4.3	3.7
90.0	1	(100)	51	61	56	5.9	5.0
			⟨011⟩ STGB:				
13.44	73	(166)		27		2.6	
31.59	27	(255)	32	38		3.7	3.1
38.94	9	(122)	38[d]	42		4.1	3.7

[a]Crack propagation along the ⟨001⟩ direction, with and without (values in brackets) conjugated bond formation.

[b]Crack propagation along the ⟨011⟩ direction, with and without (values in brackets) conjugated bond formation.

[c]Crack deviated from a (013) plane to a (001) plane.

[d]Crack deviated from the GB plane to a (111) plane.

with the Griffith evaluation using the surface energies. Detailed analysis of the dynamics revealed that this inconsistency is a result of ''π-bonding chemistry'' of bond breaking in the (110) plane. The structure of the crack tip for a crack in the (110) plane is illustrated in Fig. 7. Each step of crack propagation requires breaking bonds between two rows of atoms; the numbers 1 and 2 indicate these rows in Fig. 7. The structure of the resulting surface is such that π-bonded chains can form between atoms in the rows denoted by the numbers 2 and 3 in Fig. 7. This produces relatively low-energy surfaces created during cleavage compared to cleavage within the (111) and (100) planes. However, the potential predicts that bond rupture must be almost completed before significant energy stabilization can be realized from π-bond formation. This leads to the similar critical stress for crack propagation for this orientation relative to other low-index planes despite the other planes having higher surface energies. This effect, while qualitatively captured by the many-body features of the analytic potential, should be confirmed by first-principles-based dynamic simulations.

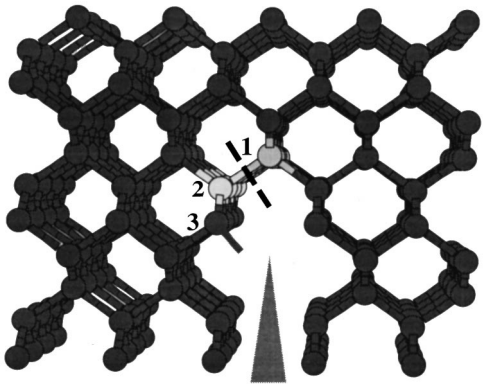

FIG. 7. Illustration of the atomic structure of a crack tip for a crack propagating along a (110) plane in the ⟨010⟩ direction.

Two directions of crack propagation, ⟨001⟩ and ⟨011⟩, have been also modeled for a crack inserted along a (110) plane. It was found that the critical stress for crack propagation in the ⟨001⟩ direction is 11% lower than that in the ⟨011⟩ direction. These two directions are not equivalent; the distance between arrays of broken bonds at each step of crack front propagation is different, as well as the relative orientation of the crack front and arrays of atoms forming π-bonded chains. Thus, simulations predict that within the same cleavage plane there can be directions with different resistances to crack propagation.

In summary, the study of bulk cleavage along low-index facets in diamond revealed that formal use of Orovan's criterion for the theoretical strength and the Griffith criterion for the critical stress of crack propagation give a ranking of the strengths for low-index facets that is inconsistent with the experimental observations. In particular, from these evaluations it follows that {011} planes should be the planes of preferred cleavage rather than {111} planes. This is due to the fact that the surface energy, used in the Orovan's and Griffith

criteria, is lowest for the {011} planes in diamond as confirmed by the DFT-LDA calculations (as well as using the bond-order potential). However, dynamic simulations, particularly with the bond-order potential, give a ranking of strengths of low-index facets that is consistent with experiment. As discussed above, this is due to the ''π-bonding chemistry'' contribution to the failure mechanisms for covalent materials with strong π bonding. In general, can be concluded that for the evaluation of the strength of covalent materials along orientations where simple bond-scission analysis can not be applied (as along the $\langle 011 \rangle$ orientation in diamond), the bond strengths should be obtained from the simulations rather than using criteria involving surface energies. Fracture modeling of diamond samples with low-index orientations using a tight-binding approach is currently in progress.

2. Individual grain boundaries

To explore the dynamics of intergranular crack propagation, a series of simulations were carried out in which a crack was inserted into a grain boundary and the system was strained in the direction perpendicular to the notch until the crack began to propagate. Two sets of simulations were run. In the first, which included a total of nine GB's at various misorientation angles, the notch was initially placed completely within the GB plane. An example of one of these simulations is illustrated in Fig. 1(b). In the second set of simulations [Fig. 1(c)], the angle of inclination of the GB plane relative to the notch plane was varied from approximately 10° to 80°, and 4–5 different configurations for each GB were modeled. The grain with a preexisting notch was oriented relative to the applied strain so that crack propagation was initiated in either in the (011) or (001) planes.

An example of one of the simulations in which the strain was applied perpendicular to the GB plane is illustrated in Fig. 1(b). The cracks propagated within the GB plane in all systems studied except the $\Sigma=9(122)$ GB for which the crack deviated to the (111) plane inclined to the (122) plane at 15°. In each case the cleavage surfaces were flat and formed without debris. Critical stresses for intergranular propagation of an initial crack 30 Å long obtained from the simulations are illustrated in Fig. 8 and summarized in Table III. For comparison, critical stresses obtained from the Griffith criterion using GB cleavage energies and Young's moduli calculated with the bond-order potential (from Table II) are also presented in Fig. 8. It is evident from the figure that the dependence of critical stress on misorientation is similar for both approaches (the maximum difference is about 20%), especially given that a variety of additional factors may influence the simulation, including system size, nonlinearity of interatomic interactions, and different tip radii. This suggests that GB cleavage energy is a major parameter defining GB resistance to crack propagation.

Critical stresses for crack propagation within GB's are about 30–40 % lower than those for an ideal crystal except for the $\Sigma=5(012)$ and $\Sigma=5(013)$ special GB's, where the maximum stresses for crack propagation are close to the stresses for crack propagation in ideal samples (Table III).

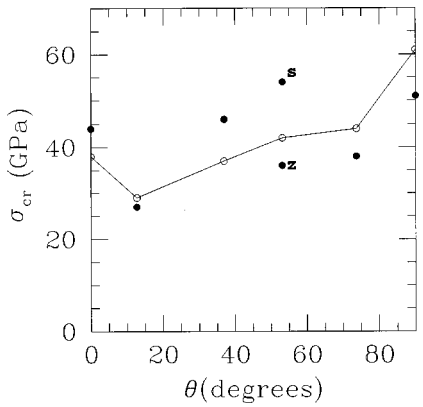

FIG. 8. Critical stresses for crack propagation within $\langle 001 \rangle$ tilt GB's obtained from molecular dynamics simulations (solid circles) and calculated from the Griffith criterion (open circles). For the $\Sigma=5(013)$ GB critical stresses for a crack propagation within two GB models with straight (*s*) and zigzag (*z*) arrangement of structural units are shown.

Critical stresses obtained in dynamic simulations for these special GB's exceed those calculated from the Griffith criterion. In addition, it was found that the critical stress for crack propagation along the $\Sigma=5(013)$ GB with a zigzag arrangement of dislocation cores is about 30% lower than that for the structure with a straight arrangement of dislocation cores.[40] The difference in GB resistance to crack propagation for these two models likely originates from the different orientation of bonds within these GB's relative to the notch. In the GB with the zigzag arrangement of structural units, the bonds are almost perpendicular to the direction of crack propagation, while in the GB with the straight arrangement of structural units bonds are more elongated along the crack plane and therefore are more resistant to bond rupture.

The second series of simulations discussed in this section were carried out to explore the possibility of a planar crack changing its path as it propagates from one grain to another. This can result in the absorption of additional energy and a resulting toughness of the polycrystalline system that is higher than single crystals. The simulation setup for this set of calculations is illustrated in Fig. 1(c). Four GB's, $\Sigma=41$, $\Sigma=5$, $\Sigma=27$, and $\Sigma=9$, have been studied.

In general, when a crack reaches a GB, it can propagate within the GB (intergranular fracture), or penetrate into the second grain (transgranular fracture). Within the second grain, the crack can keep moving in the initial direction of propagation or deviate into the easier cleavage plane. These events depend on the GB cleavage energy, relative bulk cohesive energies of the first and second grains, and the inclination angle of the GB relative to the initial crack propagation plane.[17] To maintain crack propagation as the crack transverses the boundary and deviates to the preferred cleavage plane, the applied load must be increased because there is a change of a pure mode I crack propagation to a mixed mode. This increases the toughness of the material. If the crack deflects onto a weak GB, the net resistance (toughness) increases due to an increase in the actual fracture surface area.

Figures 9 and 10 show representative snapshots of cleav-

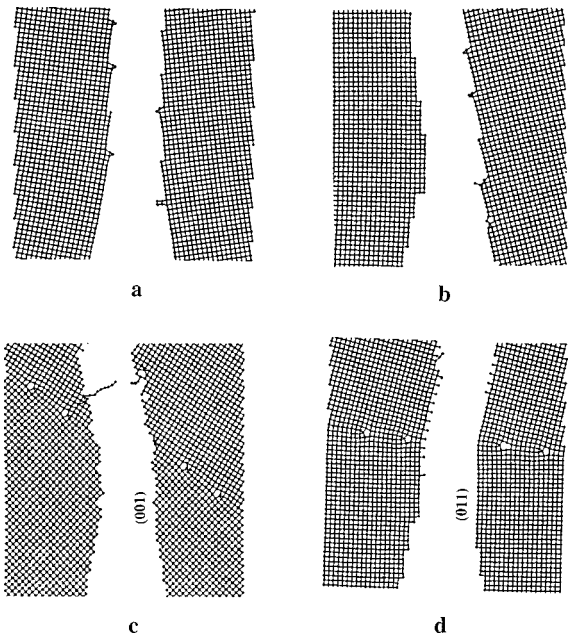

FIG. 9. Illustration of the fracture surfaces resulting from propagation of a crack inclined at different angles α to $\Sigma=41(450)$ GB plane. (a) $\alpha=0°$, $G(\alpha)/G(0)=1$, $R_0(\mathrm{GB})/R_0(\mathrm{GB})=1$; (b) $\alpha=12.7°$, $G(\alpha)/G(0)=0.97$, $R_0(\mathrm{GB})/R_0(011)=0.43$; (c) $\alpha=57.7°$, $G(\alpha)/G(0)=0.61$, $R_0(\mathrm{GB})/R_0(001)=0.32$; (d) $\alpha=77.3°$, $G(\alpha)/G(0)=0.4$, $R_0(\mathrm{GB})/R_0(011)=0.43$.

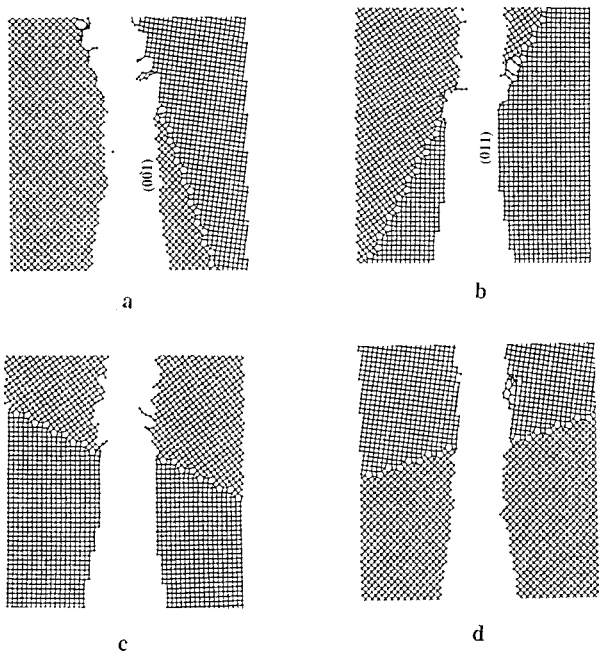

FIG. 10. Illustration of the fracture surfaces resulting from propagation of a crack inclined at different angles α to $\Sigma=5(130)Z$ GB plane. (a) $\alpha=8.1°$, $G(\alpha)/G(0)=0.95$, $R_0(\mathrm{GB})/R_0(001)=0.75$; (b) $\alpha=36.9°$, $G(\alpha)/G(0)=0.83$, $R_0(\mathrm{GB})/R_0(011)=1$; (c) $\alpha=53.1°$, $G(\alpha)/G(0)=0.6$, $R_0(\mathrm{GB})/R_0(011)=1$; (d) $\alpha=81.9°$, $G(\alpha)/G(0)=0.35$, $R_0(\mathrm{GB})/R_0(011)=0.75$.

age surfaces after crack propagation in systems with $\Sigma=41$ and $\Sigma=5\langle001\rangle$ tilt GB's. Unless an angle between a primary crack plane and a GB is small [Figs. 9(a), 9(b), and 10(a)], the crack tends to cross the GB. A simple analysis of the condition for intergranular crack propagation can be carried out following Lawn.[17] The condition for a crack initially in pure mode I to deflect into a GB in a mixed mode is[17]

$$G(\alpha)/G(0)>R_0(\mathrm{GB})/R_0(G1), \tag{3}$$

where α is the misorientation angle between the initial crack and GB planes, $R_0(\mathrm{GB})$ is the work of adhesion of the GB, $R_0(G1)$ is the bulk cleavage energy of the grain containing the initial crack propagation, and $G(\alpha)$ and $G(0)$ are mechanical-energy-release rates that depend on the angle between the crack and the direction of applied load. Values of $G(\alpha)/G(0)$ and $R_0(\mathrm{GB})/R_0(011)$ for several $\langle001\rangle$ tilt GB's as functions of GB misorientation angle θ are plotted in Fig. 11 for a crack initially propagating in an (011) plane. The value of $R_0(011)$ (the cleavage energy of (011) planes) was calculated by the Griffith formula using the critical stress obtained from a molecular-dynamics simulation of crack propagation within a (011) plane. The ratio $G(\alpha)/G(0)$, calculated for an isotropic case, was taken from reference.[17] If $R_0(\mathrm{GB})/R_0(011)$ exceeds $G(\alpha)/G(0)$ for a given GB (Fig. 11), intergranular crack propagation as the crack reaches the GB is expected. The results of molecular dynamic simulations in Figs. 9 and 10 correspond reasonably well to these rough estimations. In crystals containing $\langle011\rangle$ tilt GB's it has been observed that cracks tend to exhibit transgranular propagation mainly along (111) planes. Thus the molecular dynamic simulation results indicate predominantly a transgranular mode of fracture in polycrystalline diamond.

3. Complex microstructures

Simulated crack propagation in a system containing a network of $\langle011\rangle$ GB's is illustrated in Fig. 12. Among the GB's

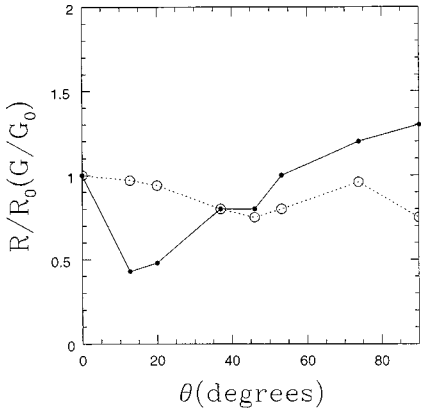

FIG. 11. Relative mechanical-energy release rate $G(\alpha)/G(0)$ (open circles) and relative crack resistance energy $R_0(\mathrm{GB})/R_0(011)$ (solid circles) as functions of GB misorientation angle θ. Calculations are carried out for a preexisting crack inserted within a (011) plane. Every GB is inclined to a preexisting crack at angle $\alpha=\min\{\theta;90°-\theta\}$.

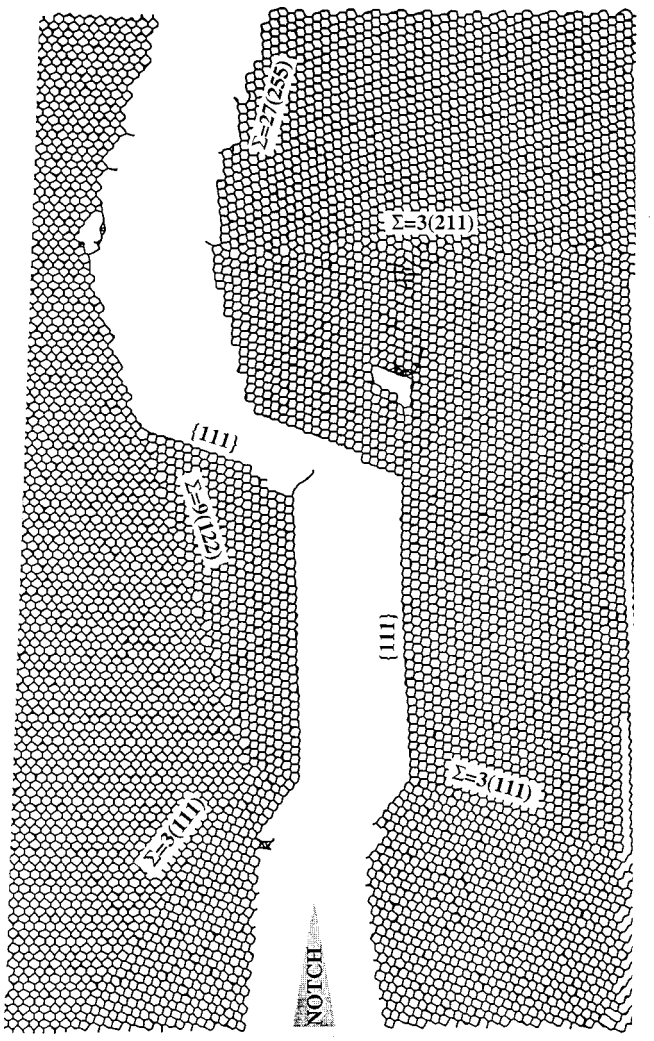

FIG. 12. Illustration of the fracture surfaces resulting from propagation of a crack in a realistic microstructure. Different initial configurations of a notch relative to the system are explored in the simulation sets.

in the system, the $\Sigma=27$ and $\Sigma=3(211)$ GB's possess the lowest cohesive energy and are therefore considered weak. In addition to a crack propagating from a notch, another crack originated at the intersection of the $\Sigma=27$ GB with a free surface (top part of Fig. 12) as applied strain was increased up to 6%. This 'top' crack intersected the triple junction and continued to propagate along the $\Sigma=9$ GB. The crack originating in the notch deviated to a (111) plane, intersected the $\Sigma=3(111)$ GB, and continued to propagate along a (111) plane until the two cracks coalesced along nother (111) plane (Fig. 12). Thus, both trans- and intergranular modes of crack propagation were observed in this set of calculations.

IV. CONCLUSIONS

Fracture strengths and resistances to crack propagation for $\langle 001\rangle$ and $\langle 011\rangle$ symmetrical tilt GB's in diamond have been studied via molecular dynamic simulations using a bond-order analytic potential. GB cleavage energies have been calculated with both density-functional theory and the bond-order potential.

It was found that the theoretical fracture stress of individual GB's is defined primarily by GB type rather than by GB cleavage energies. In particular, special GB's possess higher theoretical fracture stresses than GB's in the nearby misorientation range. The mechanism of interface failure is not that implied by the Orovan criterion, which assumes uniform distribution of the stored energy along a GB plane and therefore simultaneous breaking of all bonds along an interface. Atomistic simulations demonstrated that failure is initiated within the dislocation cores at the interface when critical local stresses are attained, and then propagated from these points along the interface.

Critical stresses for crack propagation within a GB obtained from dynamic simulations were consistent with those calculated from the Griffith criterion. Toughnesses of special GB's was about twice that of other GB's. This is in agreement with other studies and experiments on metals and ceramics.[1,11]

It was found that the chemistry of covalent materials may significantly contribute to crack propagation and therefore to failure mechanisms. In particular, the formation of π-bonded chains after crack propagation along (110) surfaces significantly reduces surface energies of (110) plane as compared to other low index planes, although the various low-index surfaces have similar stresses necessary to break the bonds. To evaluate strength properties of covalent materials along the orientations where π-bonding reconstruction is significant, the formal using of the Orovan's or Griffith criterions give incorrect strength properties. For these orientations strength properties should be obtained through, for example, dynamic simulations.

Crack propagation has been also studied in systems containing GB's of different types with different initial orientations relative to the notch. In most cases transgranular crack propagation was observed. From the balance of mechanical energy release rate and relative crack resistance of a GB and a grain, it was possible to make rough predictions of the intergranular versus transgranular crack propagation depending on GB type.

ACKNOWLEDGMENTS

Priya Vashishta, Marshall Stoneham, and Michael Frenklach are thanked for helpful discussions. O.A.S. and D.W.B. were supported by the Office of Naval Research through Contract No. N00014-95-1-0270. A.O. and X.S. were supported by the Air Force Office of Scientific Research (Grant No. F 9620-98-1-0086), USC-LSU Multidisciplinary University Research Initiative (Grant No. F 49620-95-1-0452), and the National Science Foundation (Grant No. DMR-9711903). Part of the simulations were performed on parallel machines in the Concurrent Computing Laboratory for Materials Simulations (CCLMS) at Louisiana State University. L.H.Y. was supported by the U.S. Department of Energy under Contract No. W-7405-ENG-48 at LLNL.

[1] *The Properties of Natural and Synthetic Diamond*, edited by J. E. Field (Academic, London, 1992); J. E. Field, E. Nicholson, C. R. Seward, and Z. Feng, Philos. Trans. R. Soc. London, Ser. A **342**, 261 (1993); J. E. Field and C. S. J. Pickles, Diamond Relat. Mater. **5**, 625 (1996).
[2] J. Wilks and E. Wilks, *Properties and Applications of Diamond* (Butterworth-Heinemann, Oxford, 1991).
[3] J. J. Mecholsky, Jr. and Y. L. Tsai, J. Appl. Phys. **71**, 4875 (1992).
[4] L. P. Hehn, Z. Chen, and J. J. Mecholsky, Jr., J. Mater. Res. **9**, 1540 (1994).
[5] D. S. Olson, G. J. Reynolds, G. F. Virshup, F. I. Friedlander, B. G. James, and L. D. Partain, J. Appl. Phys. **78**, 5177 (1995).
[6] G. F. Cardinale and C. J. Robinson, J. Mater. Res. **7**, 1432 (1992).
[7] M. D. Drory, R. H. Dauskardt, A. Kant, and R. O. Ritchie, J. Appl. Phys. **78**, 3083 (1995).
[8] C. S. J. Pickles, J. R. Brandon, S. E. Coe, and R. S. Sussmann, Diamond Relat. Mater. (to be published).
[9] T. Watanabe, Mater. Sci. Eng., A **176**, 39 (1994).
[10] K. T. Aust, Can. Metall. Q. **33**, 265 (1994).
[11] G. Palumbo and K. T. Aust, in *Materials Interfaces*, edited by D. Wolf and S. Yip (Chapman & Hall, London, 1992), p. 190.
[12] L. C. Lim and T. Watanabe, Acta Metall. Mater. **38**, 2507 (1990).
[13] V. Vitek, J. Phys. III **1**, 1085 (1991).
[14] S. P. Chen *et al.*, J. Mater. Res. **5**, 955 (1990); S. P. Chen, Philos. Mag. A **66**, 1 (1992); S. P. Chen, D. J. Srolovitz, and A. F. Voter, J. Mater. Res. **4**, 62 (1989).
[15] D. Wolf and J. A. Jaszczak, in *Materials Interfaces* (Ref. 11), p. 662.
[16] For example, P. Gumbsch, J. Mater. Res. **10**, 2897 (1995); M. Marder and J. Fineberg, Phys. Today **49** (9), 24 (1996); S. J. Zhou, D. M. Beazley, P. S. Lomdahl, and B. L. Holian, Phys. Rev. Lett. **78**, 479 (1997).
[17] B. Lawn, *Fracture of Brittle Solids* (Cambridge University Press, Cambridge, 1993).
[18] R. Chang, Int. J. Fract. Mech. **6**, 111 (1970).
[19] P. C. Gehlen and M. F. Kanninen, in *Inelastic Behavior of Solids*, edited by M. F. Kanninen (McGraw-Hill, New York, 1970), p. 587.
[20] J. E. Sinclair and B. R. Lawn, Proc. R. Soc. London, Ser. A **329**, 83 (1972).
[21] V. B. Shenoy *et al.*, Phys. Rev. Lett. **80**, 742 (1998).
[22] R. K. Kalia *et al.*, Phys. Rev. Lett. **78**, 2144 (1997).
[23] A. Omeltchenko, J. Yu, R. K. Kalia, and P. Vashishta, Phys. Rev. Lett. **78**, 2148 (1997).
[24] D. J. Srolovitz *et al.*, in *Materials Interfaces* (Ref. 11), p. 691.
[25] J. Hornstra, Physica (Utrecht) **25**, 409 (1959).
[26] D. Shechtman *et al.*, J. Mater. Res. **8**, 473 (1993).
[27] D. W. Brenner *et al.*, in *Computer Aided Design of High Temperature Materials*, edited by A. Pechenik, R. Kalia, and P. Vashishta (Oxford University Press, Oxford, in press).
[28] D. W. Brenner, Phys. Rev. B **42**, 9458 (1990).
[29] D. W. Brenner, O. A. Shenderova, J. Harrison, and S. Sinnott (unpublished).
[30] H. J. McSkimin and P. Andreatch, J. Appl. Phys. **43**, 2944 (1972).
[31] O. Shenderova, D. Brenner, L. H. Yang, A. Omeltchenko, and A. Nazarov, in *Diamond Materials V*, edited by J. L. Davidson *et al.*, ECS Proceedings Series (The Electrochemical Society, Pennington, NJ, 1998), p. 360.
[32] W. R. Tyson, Philos. Mag. **14**, 925 (1966).
[33] O. A. Shenderova, D. W. Brenner, A. I. Nazarov, A. E. Romanov, and L. Yang, Phys. Rev. B **57**, R3181 (1998).
[34] G. Kern and J. Hafner, Phys. Rev. B **56**, 4203 (1997).
[35] A. Kelly, *Strong Solids* (Clarendon, Oxford, 1973).
[36] J. Whitlock and A. L. Ruoff, Scr. Metall. **15**, 525 (1981).
[37] S. Ramaseshan, Proc.-Indian Acad. Sci., Sect. A **24**, 114 (1946).
[38] E. Orowan, Rep. Prog. Phys. **12**, 191 (1949).
[39] A. P. Sutton and V. Vitek, Philos. Trans. R. Soc. London, Ser. A **309**, 37 (1983).
[40] O. A. Shenderova, D. W. Brenner, and L. H. Yang, Phys. Rev. B **60**, 7043 (1999).